Bodart, J. A., & Bingham, R. J. (2019). The Impact of the Extreme 2015–2016 El Niño on the Mass Balance of the Antarctic Ice Sheet. *Geophysical Research Letters*, *46*(23), 13862-13871. https://doi.org/10.1029/2019GL084466

Geophysical Research Letters

RESEARCH LETTER
10.1029/2019GL084466

The Impact of the Extreme 2015–2016 El Niño on the Mass Balance of the Antarctic Ice Sheet

J.A. Bodart[1,2] and R.J. Bingham[2]

[1]School of GeoSciences, University of Edinburgh, Edinburgh, UK, [2]Bristol Glaciology Centre, School of Geographical Sciences, University of Bristol, Bristol, UK

Key Points:
- Precipitation-derived mass anomalies are estimated for the Antarctic Ice Sheet over the GRACE period
- An unprecedented increase in accumulation over the Antarctic Peninsula and West Antarctica coincides with the extreme 2015–2016 El Niño
- This was sufficient to temporarily offset Antarctica's usual (≈0.4 mm yr^{-1}) contribution to global mean sea level rise

Supporting Information:
- Supporting Information S1

Correspondence to:
J. A. Bodart,
julien.bodart@ed.ac.uk

Citation:
Bodart, J. A., & Bingham, R. J. (2019). The impact of the extreme 2015–2016 El Niño on the mass balance of the Antarctic ice sheet. *Geophysical Research Letters*, *46*, 13,862–13,871. https://doi.org/10.1029/2019GL084466

Received 10 JUL 2019
Accepted 14 NOV 2019
Accepted article online 19 NOV 2019
Published online 4 DEC 2019
Corrected 15 JAN 2020

This article was corrected on 15 JAN 2020. See the end of the full text for details.

Abstract Interannual variations associated with El Niño-Southern Oscillation can alter the surface-pressure distribution and moisture transport over Antarctica, potentially affecting the contribution of the Antarctic ice sheet to sea level. Here, we combine satellite gravimetry with auxiliary atmospheric data sets to investigate interannual ice-mass changes during the extreme 2015–2016 El Niño. Enhanced precipitation during this event contributed positively to the mass of the Antarctic Peninsula and West Antarctic ice sheets, with the mass gain on the peninsula being unprecedented within GRACE's observational record. Over the coastal basins of East Antarctica, the precipitation-driven mass loss observed in recent years was arrested, with pronounced accumulation over Terre Adélie dominating this response. Little change was observed over Central Antarctica where, after a brief pause, enhanced mass-loss due to weakened precipitation continued. Overall, precipitation changes over this period were sufficient to temporarily offset Antarctica's usual (approximately 0.4 mm yr^{-1}) contribution to global mean sea level rise.

Plain Language Summary Given that the Antarctic Ice Sheet has the potential to raise sea level by over 50 m if completely melted, it is crucial that we fully understand the factors controlling its stability. Presently, changes in rates of mass loss and mass gain over the ice sheet vary from short (seasonal/interannual) to long (decadal) timescales. Previous research has shown that one potential factor influencing Antarctica on interannual timescales is the El Niño-Southern Oscillation, a large-scale interaction between the Pacific Ocean and the overlying atmosphere that fluctuates between warm (El Niño) and cold (La Niña) states every 2–7 years. Here, we show an unprecedented increase in accumulation over the Antarctic Peninsula and West Antarctic sectors during the extreme 2015–2016 El Niño, along with a brief stabilization in mass loss over East Antarctica. Overall, precipitation changes during this event were sufficient to temporarily offset Antarctica's usual (approximately 0.4 mm yr^{-1}) contribution to global mean sea level rise.

1. Introduction

Mass loss from glaciers and ice sheets has been one of the dominant drivers of global mean sea level (GMSL) rise since the midtwentieth century, respectively, contributing 0.86 and 0.60 mm yr^{-1} of the total observed GMSL rise of 3.2 mm yr^{-1} for the period 1993–2010 (IPCC AR5, 2013). Antarctica's continent-wide ice-mass discharge between 1992 and 2017 is estimated to have been 109 ± 56 Gt yr^{-1}, equivalent to 7.06 ± 3.9 mm of GMSL rise (Shepherd et al., 2018). However, mass change over the Antarctic Ice Sheet (AIS) is not uniform, instead exhibiting strong regional variations, with much greater mass loss from West Antarctica (94 ± 27 Gt yr^{-1}) and the Antarctic Peninsula (20 ± 15 Gt yr^{-1}), compared with a mass gain over East Antarctica (5 ± 46 Gt yr^{-1}) over the same period (1992–2017; Shepherd et al., 2018).

Regional mass variations occur on interannual to decadal timescales. When estimating decadal mass rates over individual regions, the Antarctic Peninsula and West Antarctica exhibit negative mass trends dominated by glacial discharge from melting and calving events of large ice streams and ice shelves (Gardner et al., 2018; Holland et al., 2010; Mouginot et al., 2014; Rignot et al., 2013), whereas East Antarctica has experienced a slight mass gain due in part to an increase in precipitation rates (Medley et al., 2018; Shepherd et al., 2012; Shepherd et al., 2018). In addition, mass change over the ice sheet is also affected by climate-driven interannual fluctuations, such as those associated with El Niño-Southern Oscillation (ENSO).

As the dominant and most far-reaching mode of interannual climate variability, the impact of ENSO on the AIS is of particular interest. El Niño's influence in the Southern Hemisphere's high latitudes has been associated with blocking events induced by Rossby wave trains that alter surface-pressure distribution and

moisture transport over the Amundsen Sea (Chen et al., 1996; Cullather et al., 1996; Sasgen et al., 2010; Turner, 2004). The effect of ENSO on Antarctica has also been associated with anomalies in sea surface temperature and sea ice extent (Kwok et al., 2016; Pope et al., 2017), ice-shelf thinning rates (Deb et al., 2018; Paolo et al., 2018; Walker & Gardner, 2017), and surface melt events (Scott et al., 2019; Tedesco & Monaghan, 2009). Boening et al. (2012) showed that the presence of a seesaw pattern of high and low pressure systems over Dronning Maud Land following the 2009–2010 El Niño led to increased cloud formation and subsequent precipitation in this sector. This resulted in an additional 350 Gt of cumulative mass gain in this sector, equivalent to a decrease of 0.32 mm yr^{-1} in GMSL between 2009 and 2011 (Boening et al., 2012).

Compared with the relatively moderate 2009 El Niño, the 2015–2016 El Niño was one of the strongest on record, with sea surface temperature anomalies in the Pacific exceeding 2.5 °C. This event has already been linked with the lowest Southern Hemisphere spring sea ice extent ever recorded (Stuecker et al., 2017), widespread and long-lasting surface melting over the Ross Ice Shelf (Nicolas et al., 2017), and intense calving activity in East Antarctica (Aoki, 2017). In light of the magnitude and wide-reaching impacts of this event, we consider here its effect on the mass balance of the AIS. Section 2 of this paper describes the data sets and methods used. Section 3 shows the results for the observed mass changes (section 3.1) and associated atmospheric drivers (section 3.2). Finally, section 4 provides a concluding discussion.

2. Data Sets and Methods

2.1. GRACE Mascons

GRACE RL06M mascon solutions from the Jet Propulsion Laboratory (https://grace.jpl.nasa.gov/data/get-data/jpl_global_mascons) spanning the period 2002–2017 are used to estimate interannual mass variability over the AIS. The mascon solution is obtained by fitting 4,551 equal-area 3° spherical cap functions directly to the intersatellite range-rate measurements and is provided on a 0.5° × 0.5° global grid in terms of equivalent water height. Geophysically based a priori constraints obviate the need to apply empirical destriping or smoothing algorithms, as is required for conventional spherical harmonic solutions (Luthcke et al., 2013; Watkins et al., 2015). A version of the data set employing a coastline resolution improvement filter to improve the separation of land and ocean mass signals (Watkins et al., 2015; Wiese et al., 2016) was found to underestimate mass change in some basins of the Antarctic Peninsula (see supporting information Figures S1 and S2). Therefore, we use the version without this additional postprocessing.

To examine interannual mass variations of the AIS at regional and basin scales, the gridded mascon solutions were integrated over each mascon window to restore the data to its original resolution. The fraction of each mascon lying within the 27 drainage basins defined by Zwally et al. (2012; http://icesat4.gsfc.nasa.gov/cryo_data/ant_grn_drainage_systems.php; Figure 1), and the oceanic zone beyond the grounding line, was then determined, and the mass within each basin summed accordingly. For mascons occupying multiple basins, their mass was distributed to the basins in proportion to the fraction of their area lying within each basin. Similarly, for land/ocean mascons, the fraction of their area/mass lying over the ocean was redistributed to the other basins over which they lie in proportion to their fractional occupation of these basins. This assumes that for these mascons, the ocean makes a negligible contribution to the total mass; a reasonable assumption at the interannual timescales considered here. However, a more conservative (lower-bound) estimate where the ocean component of the mascon is not redistributed (effectively assuming the ocean and land contributions are of equal magnitude) has little impact on our analysis (see Figures S1 and S2).

Individual basins were then combined into four AIS regions: the West AIS (WAIS; Basins 1 and 18–23), the Antarctic Peninsula Ice Sheet (APIS; Basins 24–27), the East AIS (EAIS; Basins 4–9 and 11–16), and the Central AIS (CAIS; Basins 2, 3, 10, and 17) (Figure 1). The definition of the CAIS as distinct from the EAIS is motivated by opposing geophysical conditions over the eastern AIS, with higher altitude and drier conditions over the Antarctic interior (CAIS) compared to the low-lying, accumulation-prone coastal basins of the EAIS (Lenaerts et al., 2012; Palerme et al., 2014). To facilitate comparison to previous studies where this separation is not made, values for the entire EAIS are also provided in Table S1.

Since our focus is on interannual variability, all time series were detrended, thereby eliminating any impact of the Glacial Isostatic Adjustment signal or correction, and seasonal and intra-annual variability was

Figure 1. Regional distribution of basin numbers (1–27), with the West Antarctic Ice Sheet (red), the Antarctic Peninsula Ice Sheet (yellow), the East Antarctic Ice Sheet (green), and then Central Antarctic Ice Sheet (blue).

removed by subtracting the mean seasonal cycle and applying a boxcar filter of length 13 months. Occasionally, a GRACE monthly solution is formed from observations spanning two adjacent months. In such cases, the monthly solution is aligned to the month in which the majority of the observations lie. For some months where there is no GRACE solution, data gaps are filled by the mean of the surrounding months within the 13 month boxcar window. Information on the uncertainty estimates for the GRACE time series can be found in the supporting information.

2.2. Meteorological Fields

To assess the atmospheric drivers of the interannual mass variations observed by GRACE, we used ECMWF's ERA-Interim (Dee et al., 2011) and the recently released ERA5 (Hersbach & Dee, 2016) reanalysis products, NASA's MERRA-2 reanalysis product (Gelaro et al., 2017), together with output from the MAR (Version 3.6.4) Regional Climate Model (RCM) (Agosta et al., 2019) for which we summed the snowfall and rainfall and subtracted the sublimation, and the RACMO2 (Version 3.2) RCM (van Wessem et al., 2018). We calculated net precipitation from the ERA products by subtracting evaporation/sublimation from the total precipitation but found that this had little impact on the results. All fields were filtered following the approach outlined above for the GRACE data.

To enable a direct comparison between the GRACE and the net precipitation fields, the latter were integrated over the GRACE period and then detrended so that the resulting time series reflected variations in mass due to fluctuations in the precipitation rate relative to the mean rate. Thus, positive mass anomalies represent a period of elevated precipitation relative to the mean rate over the GRACE period. Conversely, negative mass anomalies represent a period of weakened precipitation. These time series were then low-pass filtered in the same fashion as outlined above for the GRACE data. Finally, basin and regional time series of precipitation-driven mass change were obtained by integration over the basins defined above and the five estimates averaged to give a single estimate for each region/basin. This mean precipitation-mass estimate (M_P) most closely matched the GRACE total-mass estimate (M_T), accounting for 77% of the total variance

(henceforth referred to as skill) in the GRACE basin-scale time series, compared with 76% (ERA-Interim), 75% (ERA5), 72% (RACMO2), 70% (MERRA-2), and 64% (MAR) for the individual time series.

3. Results

3.1. Observed Mass Changes

Although differing somewhat in their details, the overall correspondence between the M_T and M_P time series seen in Figure 2a demonstrates that interannual mass fluctuations over the AIS are mainly driven by precipitation, with M_P accounting for 79% of the variance in M_T. According to GRACE, between February 2012 and May 2015, the AIS lost an additional 341 ± 33 Gt of mass relative to the long-term rate. This compares with 260 ± 36 Gt from M_P, suggesting the enhanced mass loss was driven primarily by weaker than average precipitation over this period (errors calculated as described in the supporting information). This trend reversed sharply in mid-2015, when both the M_T and M_P time series reach a minimum. Between June

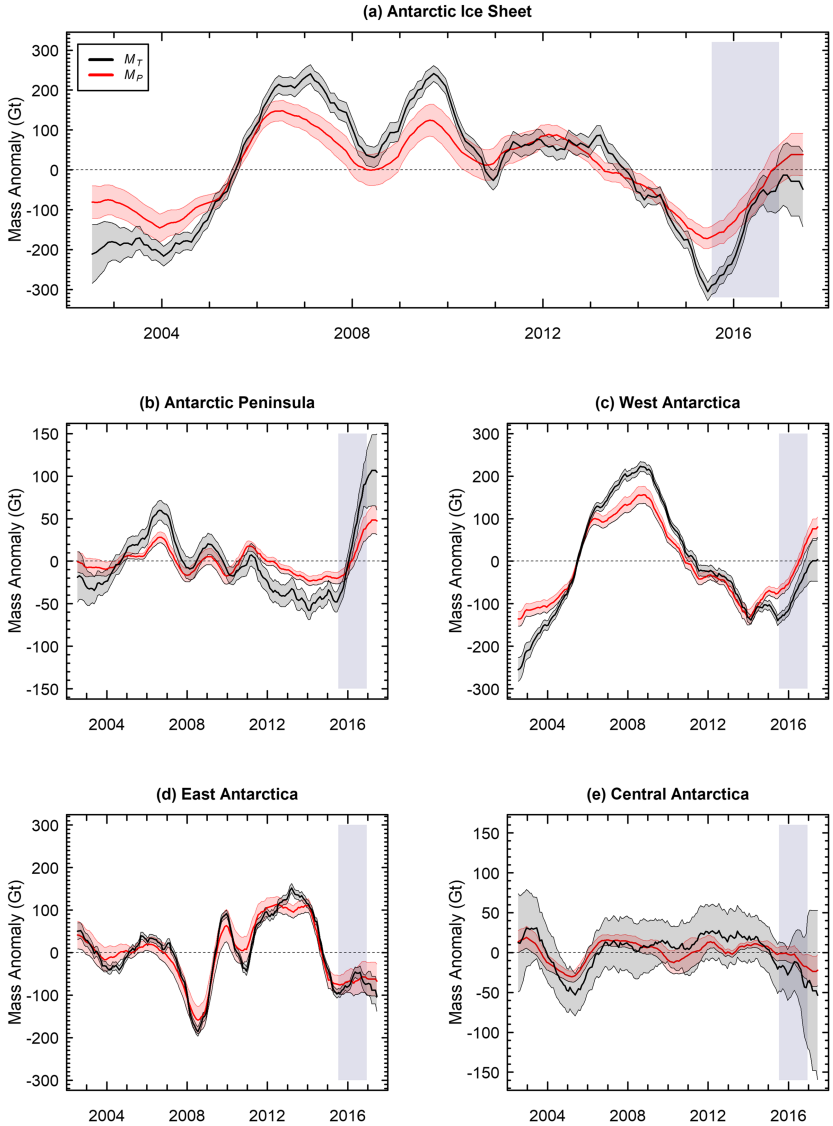

Figure 2. Interannual variations in total mass (M_T) from GRACE (black) and precipitation-driven mass (M_P) derived from an average of the ERA and MERRA-2 reanalysis products, and the MAR and RACMO2 regional climate models (red): (a) Antarctic Ice Sheet, (b) Antarctic Peninsula, (c) West Antarctica, (d) East Antarctica, and (e) Central Antarctica. The shading represents 95% confidence intervals. The blue-shaded box represents the El Niño period July 2015 to December 2016.

2015 and March 2017, higher than average precipitation lead to an increase in mass of 210 ± 59 Gt according to M_P, with M_T showing a larger gain of 277 ± 91 Gt, with respect to the long-term trend.

This mass gain coincides with the exceptionally strong 2015 El Niño (henceforth EN15). According to the Oceanic Niño Index (ONI; obtained from NOAA's Climate Prediction Centre: http://www.cpc.ncep.noaa.gov), EN15 began in November 2014 (ONI > 0.5 °C), reached its peak in December 2015 (ONI = 2.6 °C), and ended in May 2016. The AIS mass gain begins in June 2015, the month after which the ONI first exceeds 1.0 °C, consistent with a lagged response to ENSO at polar latitudes (e.g., Sasgen et al., 2010).

Relative to the typical amplitude of interannual fluctuations, the increase in mass during EN15 is most pronounced for the APIS (Figure 2b). This is true of both the M_T and M_P time series but with the relative mass gain during EN15 in M_T (155 ± 44 Gt) being more than twice that seen in M_P (69 ± 18 Gt). Given the relatively coarse spatial resolution of the mascons and the uniformity assumption we have effectively made when redistributing the mascon mass between basins, the basin-scale time series (Figure 3 and Table S1) for the APIS must be treated with caution. However, it is clear that the APIS mass gain can be attributed primarily to Basin 24, the largest of the APIS basins (M_T = 87 ± 18 Gt; M_P = 52 ± 14 Gt). It seems reasonable to assume, given the meteorological conditions associated with EN15 (see below), that the mass increases seen by GRACE in Basins 26 and 27 on the eastern side of the peninsula in fact originate in Basins 25 and 24, respectively. Given the absence of an EN15 response in Basin 26 for M_P, reallocating the mass from Basin 26 to Basin 25, further accentuates the difference between M_T and M_P in Basin 25, with M_T showing a mass gain during EN15 of 50 ± 15 Gt compared with 13 ± 9 Gt from M_P. Similarly, reallocating the mass changes in Basin 27 extends the difference between M_T and M_P in Basin 24 (M_T = 105 ± 27 Gt; M_P = 55 ± 18 Gt).

A similar picture emerges for the WAIS (Figure 2c), with both M_T and M_P showing mass gain during EN15, terminating a number of years of enhanced mass loss, but with the amplitude of the gain seen in M_P (152 ± 26 Gt) greater than that in M_T (141 ± 50 Gt). Figure 3 shows this mass gain can be attributed mainly to Basins 1 (M_T = 41 ± 91 Gt; M_P = 33 ± 16 Gt), 22 (M_T = 24 ± 70 Gt; M_P = 32 ± 11 Gt), and 23 (M_T = 23 ± 20 Gt; M_P = 21 ± 7 Gt). Although, Basin 20 (M_T = 24 ± 44 Gt; M_P = 29 ±13 Gt) gains more mass than Basin 23 during EN15, this appears to be part of a longer-term trend of enhanced precipitation, rather than a reversal of phase associated with EN15.

For the EAIS and CAIS, the response to EN15 is more nuanced. Unlike the APIS and the WAIS, there is little net change in mass over (coastal) East Antarctica during EN15 (Figure 2d). However, an increase in precipitation during EN15 arrested the enhanced mass loss due to relatively weak precipitation in the preceding 2–3 years. At the basin level, there is a range of responses. Basin 14 on the Terre Adélie coast gains mass during EN15, with M_P and M_T giving gains of 52 ± 14 and 62 ± 84 Gt, respectively. Its smaller neighbor, Basin 15, also gains mass (M_T = 15 ± 18 Gt; M_P = 20 ± 8 Gt) during EN15. In this case, however, the increase begins in December 2014, several months earlier than the increases in other basins, coinciding, according to the ONI, with the onset of EN15. Basins 5 and 6 on the Dronning Maud Land coast also show some mass gain during EN15, but, unlike Basins 14 and 15, this appears relatively short lived. For the remaining basins, the enhanced mass loss due to drier conditions seen in the preceding years generally continues through EN15. For some basins, there is an initial period where the enhanced mass loss is halted around the peak of EN15, before resuming again during 2016, while for others, there is a less dramatic but sustained reduction in the rate of enhanced mass loss.

The poorest agreement between M_P and M_T is seen over the CAIS, with M_P failing to capture the magnitude of the enhanced mass loss seen in the GRACE record beginning in June 2013 and continuing through EN15 (Figure 2e). Between June 2014 and March 2017, the mass loss according to M_T is −68 ± 104 Gt compared with −35 ± 19 Gt from M_P. Similar to the response in some of the EAIS basins, EN15 onset seems associated with a brief respite from the ongoing mass loss. This form of response is seen most clearly in Basins 3 and 10 but with the loss resuming at a somewhat greater rate in the latter basin (Figure 3). In contrast, Basin 2 shows a positive but unsustained response to EN15, similar to that seen in some of the EAIS basins. For Basin 17, the result is somewhat inconclusive, with M_T showing the aforementioned pause in enhanced mass loss associated with EN15, while M_P shows a more sustained mass gain starting in September 2016.

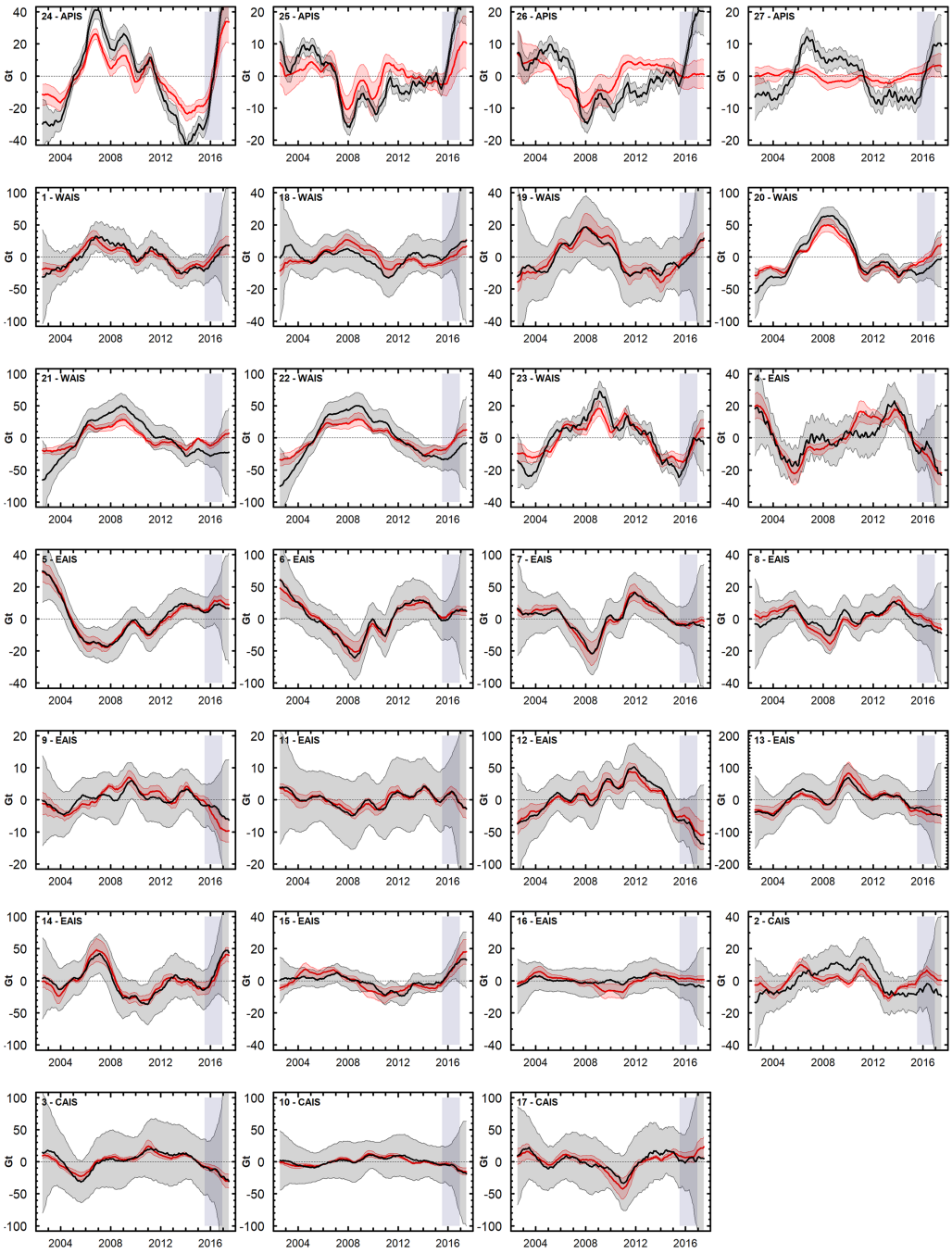

Figure 3. Interannual variations in total mass (M_T) from GRACE (black) and precipitation-driven mass (M_P) derived from an average of the ERA and MERRA-2 reanalysis products and the MAR and RACMO2 regional climate models (red) for each of the individual drainage basins defined by Zwally et al. (2012; see Figure 1). The shading represents 95% confidence intervals. The blue-shaded box represents the El Niño period July 2015 to December 2016.

3.2. Associated Atmospheric Drivers

The prevailing atmospheric conditions over the AIS and Southern Ocean are dominated by a zonally symmetric flow (westerly jet), as illustrated by the contours of absolute mean sea level pressure (MSLP) in Figure 4a. In the year preceding the EN15 peak, pressure is anomalously low over Antarctica (Figure 4a), indicative of a positive phase of the Southern Annular Mode and enhanced westerly winds. The strengthened flow remains (or is even more so) oriented parallel to the Antarctic coastline, resulting in less moist

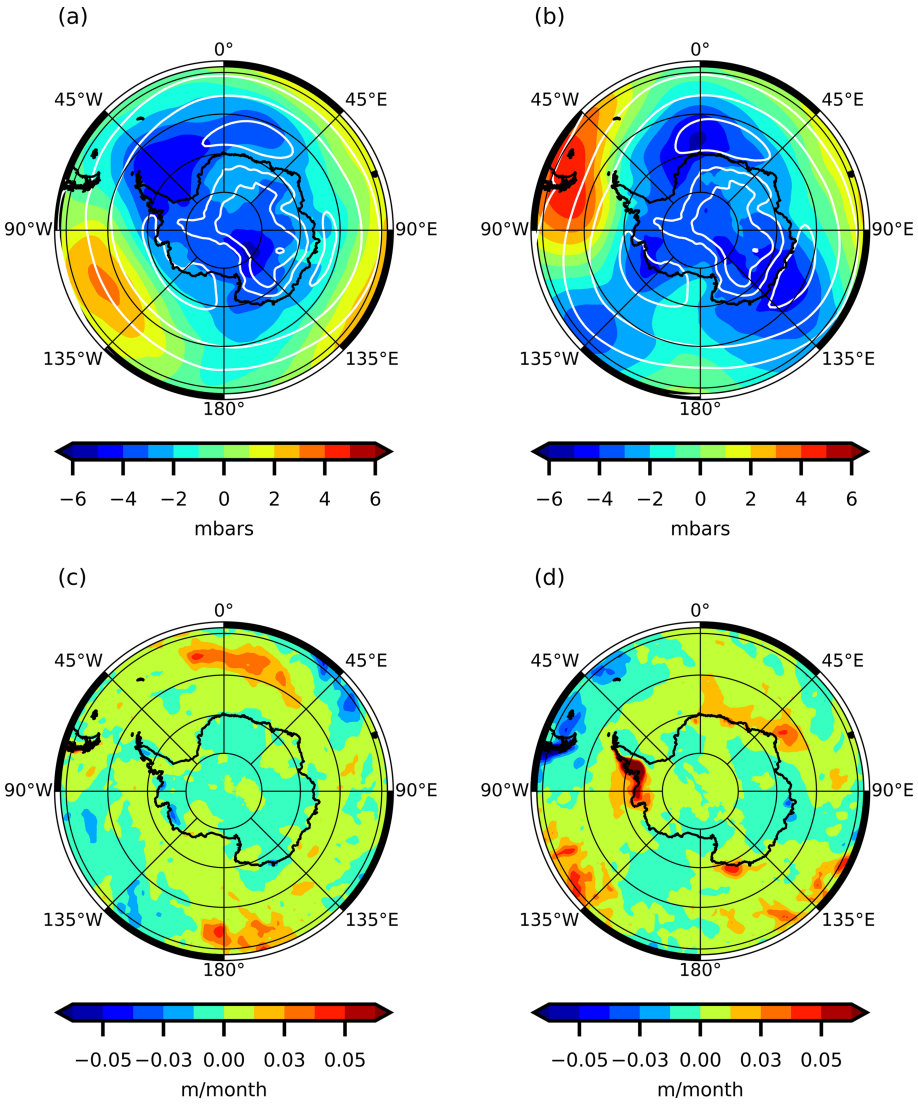

Figure 4. Pre (November 2014 to October 2015) and post (November 2015–October 2016) peak El Niño yearly means of mean sea level pressure (MSLP) and total precipitation (TP) from ERA-interim: (a) MSLP pre-El Niño, (b) MSLP post-El Niño, (c) TP pre-El Niño, and (d) TP post-El Niño.

air and associated precipitation reaching the AIS (Figure 4c). This is consistent with the enhanced mass loss seen in the years preceding EN15 seen in Figure 2a.

During EN15, a distinct zonal wave number 3 (Karoly, 1989) pattern emerges, manifest clearly in the absolute MSLP contours shown in Figure 4b. In the anomalous MSLP field, this wave appears as the tri-pole of low pressure areas located approximately at 0°E, 135°E, and 135°W. Pressure is higher between these lows, especially over the tip of South America (Figure 4b). With the resulting deviation of the westerly flow from its previously more strongly zonal orientation and the southward shift in winds associated with the anomalous high over South America, warm moist air is brought more readily onto the continent. In Figure 4d, this is seen most clearly along the Amundsen coast, consistent with the increases in mass seen in Figures 2 and 3 for the APIS and WAIS. Enhanced precipitation associated with the anomalous circulation is also clear along the Dronning Maud Land and Terre Adélie coastlines of the EAIS, again consistent with the observed mass increases in Basins 5 and 6 and Basins 14 and 15 (Figure 3). Over much of the remainder of the AIS, precipitation remains anomalously low, as is the case over much of the EAIS, or is slightly elevated, as over some of the CAIS basins, with the net effect that the overall response of the AIS to EN15 is positive.

4. Concluding Discussion

The combined analysis of GRACE, the ERA and MERRA-2 reanalyses products, and the MAR and RACMO2 RCMs shows that enhanced precipitation over Antarctica during EN15 reversed a period of enhanced mass loss due to weaker than average precipitation, with the increased precipitation contributing around 210 ± 59 Gt to the mass of the AIS between June 2015 and March 2017. This net gain can be attributed to increased precipitation over the APIS (69 ± 18 Gt) and the WAIS (152 ± 26 Gt), particularly along the Bellingshausen Sea coast (Basins 23 and 24) and the Pine Island Glacier (Basins 1 and 22). Basins 14 and 15 on the Terre Adélie coast of the EAIS contributed an additional 72 ± 16 Gt. The remaining basins either showed a temporary small increase or reduction in the rate of mass loss, before continuing their original downward trajectory.

To put this change in the context of the long-term trend of mass loss, over the period March 2006 to June 2015, the AIS lost mass at a rate of 154 Gt yr^{-1}, equivalent to 0.4 mm yr^{-1} of sea level rise. In contrast, from June 2015 to March 2017, the AIS gained mass at a rate of 67 Gt yr^{-1}, equivalent to a fall in sea level of 0.2 mm yr^{-1}. Even taking the lower M_P estimate of mass gain over the APIS, the mass gain due to enhanced precipitation during EN15 was sufficient to offset the AIS contribution to sea level rise from other processes.

The rate and magnitude of the increase in mass over the AIS as a whole is not exceptional, being comparable to that seen near the beginning of the record from December 2003 to May 2006 (Figure 2a). However, this increase coincided with a period when the ONI went from weakly positive to weakly negative. Moreover, the other two periods of increase occurred during weakly negative phases of ENSO. Thus, from this analysis alone, it is not yet possible to make a robust link between ENSO and precipitation-driven fluctuations in the net mass of the AIS. Nonetheless, the magnitude of the increases seen in the aforementioned basins is exceptional over the period, particularly over the APIS region. This is consistent with EN15 being the strongest El Niño event over the GRACE period.

According to the ERA-interim reanalysis, the increase in mass seen over the Bellingshausen Sea coastal basins of the APIS and WAIS is driven by the development of a strong zonal wave number 3 pattern which directs warm, moist air onto the continent from lower latitudes. This is consistent with Karoly (1989) and Yuan and Li (2008) who describe a similar pattern over the AIS during El Niño years. Yet, despite the 1997–1998 El Niño being the strongest ENSO event of the twentieth century, there is no clear presence of a zonal wave number 3 pattern and corresponding precipitation increases following this event (Figure S3). This shows that although there is a well-established link between ENSO and atmospheric conditions over Antarctica, for which this study provides further evidence, increased precipitation, of the form seen during EN15, is not a necessary feature of extreme El Niño events. This is not surprising. Just as no two El Niño events are identical nor will be their impact over the AIS. Moreover, the precise impact is likely modulated by local conditions such as the state of the zonal wind field as reflected by the Southern Annular Mode (Fogt & Bromwich, 2006; Nicolas et al., 2017).

Compared with the reanalysis- and RCM-based precipitation estimate (69 ± 18 Gt), GRACE gives a much larger estimate (155 ± 44 Gt) of the mass gain by the APIS during EN15. The estimates fail to agree even within their error bars. And even the largest precipitation estimate of 88 Gt, given by the ERA-Interim reanalysis is considerably less than that given by GRACE. It is hard to give a definitive answer to why this might be. While a deficiency in the mascon product cannot be ruled out, given the important role played by orography in driving the precipitation over the peninsula (van de Berg & Medley, 2016) and the sensitivity of orographic precipitation to horizontal resolution (e.g., Genthon et al., 2009; Smith et al., 2015), a plausible explanation is that the limited ability of the relatively coarse-resolution models to resolve the features and dynamics of the Antarctic Peninsula leads them to underestimate the true accumulation during EN15. This might be further exacerbated by the sparse in situ observations over the APIS.

Apart from the APIS, the most notable difference between M_T and M_P is the fact that the latter gives an 11 Gt larger increase in mass over the WAIS during EN15. This is not a significant difference when the uncertainty bounds are considered. A possible explanation, however, is that another dynamical process begins or accelerates in June 2016, offsetting the mass gain from increased precipitation. One such process could be elevated ice-shelf basal melting and discharge of grounded ice, perhaps triggered by enhanced ocean upwelling in response to the anomalous atmospheric conditions associated with EN15.

Indeed, Paolo et al. (2018) find increased thinning of the Pacific-sector ice shelves of Antarctica, particularly in the Amundsen Sea sector during EN15. Consistent with the hypothesis that such thinning could lead to enhanced grounded-ice discharge, offsetting to some extent the mass gain due to increased precipitation, it is for those WAIS basins (20–22) discharging into the Amundsen Sea where we find that the M_P mass gain is greater than that given by M_T, with, in contrast, good agreement in the other basins (see Table S1).

Finally, it must be acknowledged that the precipitation-driven fluctuations in Antarctica's ice mass balance as shown here represent relatively short-duration modulations of the much longer-term trend of ongoing net mass loss from the AIS and associated sea level rise. Indeed, irrespective of whether extreme ENSO events such as EN15 become more common in the future (e.g., Cai et al., 2014; Lee & McPhaden, 2010), they would likely offer little cumulative resistance against other factors driving enhanced mass loss. Nonetheless, for a full understanding of the response of the AIS to future climate change, the potential cumulative impact of future ENSO events are certainly worthy of further investigation.

Acknowledgments

J. A. B was supported by the NERC Doctoral Training Partnership Grant (NE/L002558/1), hosted in the Edinburgh E3 DTP program. We would like to acknowledge NASA for making the GRACE Mascon solutions (https://grace.jpl.nasa.gov/data/get-data/jpl_global_mascons) and the MERRA-2 data (https://gmao.gsfc.nasa.gov/reanalysis/MERRA-2) freely accessible online, as well as the ECMWF for the ERA reanalysis products (https://www.ecmwf.int/en/forecasts/datasets). We also thank Agosta and Fettweis for providing the MAR output product (https://zenodo.org/record/2547638) and Michiel van den Broeke for providing the RACMO2 product (contact: m.r.vandenbroeke@uu.nl). Data from this study are available at the University of Bristol data repository, data.bris, at: https://doi.org/10.5523/bris.2246mkya74pjh21yqh9ear4s4z. We thank Mathieu Morlighem and two anonymous reviewers for providing detailed comments that helped to improve the manuscript.

References

Agosta, C., Amory, C., Kittel, C., Orsi, A., Favier, V., Gallée, H., et al. (2019). Estimation of the Antarctic surface mass balance using the regional climate model MAR (1979–2015) and identification of dominant processes. *The Cryosphere*, *13*(1), 281–296. https://doi.org/10.5194/tc-2018-76

Aoki, S. (2017). Breakup of land-fast sea ice in Lützow-Holm Bay, East Antarctica, and its teleconnection to tropical Pacific sea surface temperatures. *Geophysical Research Letters*, *44*, 3219–3227. https://doi.org/10.1002/2017GL072835

Boening, C., Lebsock, M., Landerer, F., & Stephens, G. (2012). Snowfall-driven mass change on the East Antarctic Ice Sheet. *Geophysical Research Letters*, *39*, L21501. https://doi.org/10.1029/2012GL053316

Cai, W., Borlace, S., Lengaigne, M., Van Rensch, P., Collins, M., Vecchi, G., et al. (2014). Increasing frequency of extreme El Niño events due to greenhouse warming. *Nature Climate Change*, *4*(2), 111–116. https://doi.org/10.1038/NCLIMATE2100

Chen, B., Smith, S. R., & Bromwich, D. H. (1996). Evolution of the tropospheric split jet over the South Pacific Ocean during the 1986–89 ENSO cycle. *Monthly Weather Review*, *124*(8), 1711–1731. https://doi.org/10.1175/1520-0493(1996)124<1711:EOTTSJ>2.0.CO;2

Cullather, R. I., Bromwich, D. H., & Van Woert, M. L. (1996). Interannual variations in Antarctic precipitation related to El Niño-Southern Oscillation. *Journal of Geophysical Research*, *101*(D14), 19,109–19,118. https://doi.org/10.1029/96JD01769

Deb, P., Orr, A., Bromwich, D. H., Nicolas, J. P., Turner, J., & Hosking, J. S. (2018). Summer drivers of atmospheric variability affecting ice shelf thinning in the Amundsen Sea Embayment, West Antarctica. *Geophysical Research Letters*, *45*(9), 4124–4133. https://doi.org/10.1029/2018GL077092

Dee, D. P., Uppala, S. M., Simmons, A. J., Berrisford, P., Poli, P., Kobayashi, S., et al. (2011). The ERA-Interim reanalysis: Configuration and performance of the data assimilation system. *Quarterly Journal of the Royal Meteorological Society*, *137*(656), 553–597. https://doi.org/10.1002/qj.828

Fogt, R. L., & Bromwich, D. H. (2006). Decadal variability of the ENSO teleconnection to the high-latitude South Pacific governed by coupling with the southern annular mode. *Journal of Climate*, *19*(6), 979–997. https://doi.org/10.1175/JCLI3671.1

Gardner, A. S., Moholdt, G., Scambos, T., Fahnstock, M., Ligtenberg, S., van den Broeke, M., & Nilsson, J. (2018). Increased West Antarctic and unchanged East Antarctic ice discharge over the last 7 years. *The Cryosphere*, *12*(2), 521–547. https://doi.org/10.5194/tc-12-521-2018

Gelaro, R., McCarty, W., Suárez, M. J., Todling, R., Molod, A., Takacs, L., et al. (2017). The modern-era retrospective analysis for research and applications, version 2 (MERRA-2). *Journal of Climate*, *30*(14), 5419–5454. https://doi.org/10.1175/JCLI-D-16-0758.1

Genthon, C., Krinner, G., & Castebrunet, H. (2009). Antarctic precipitation and climate-change predictions: Horizontal resolution and margin vs plateau issues. *Annals of Glaciology*, *50*(50), 55–60. https://doi.org/10.3189/172756409787769681

Hersbach, H., & Dee, D. (2016). *ERA-5 Reanalysis is in production*. ECMWF Newsletter, Number 147 (p. 7). Reading, UK: ECMWF.

Holland, P. R., Jenkins, A., & Holland, D. M. (2010). Ice and ocean processes in the Bellingshausen Sea Antarctica. *Journal of Geophysical Research*, *115*(C5), C05020. https://doi.org/10.1029/2008JC005219

IPCC AR5 (2013). In T. F. Stocker, D. Qin, G.-K. Plattner, M. Tignor, S. K. Allen, J. Boschung, A. Nauels, Y. Xia, V. Bex, & P. M. Midgley (Eds.), *Climate change 2013: The physical science basis. Contribution of Working Group I to the Fifth Assessment Report of the Intergovernmental Panel on Climate Change* (p. 1535). Cambridge, UK and New York, NY, USA: Cambridge University Press. https://doi.org/10.1017/CBO9781107415324

Karoly, D. J. (1989). Southern hemisphere circulation features associated with El Niño-Southern Oscillation events. *Journal of Climate*, *2*(11), 1239–1252. https://doi.org/10.1175/1520-0442(1989)002<1239:SHCFAW>2.0.CO;2

Kwok, R., Comiso, J. C., Lee, T., & Holland, P. R. (2016). Linked trends in the South Pacific sea ice edge and Southern Oscillation Index. *Geophysical Research Letters*, *43*, 10–295. https://doi.org/10.1002/2016GL070655

Lee, T., & McPhaden, M. J. (2010). Increasing intensity of El Niño in the central-equatorial Pacific. *Geophysical Research Letters*, *37*, L14603. https://doi.org/10.1029/2010GL044007

Lenaerts, J. T. M., Den Broeke, M. R., Berg, W. J., Meijgaard, E. V., & Kuipers Munneke, P. (2012). A new, high-resolution surface mass balance map of Antarctica (1979–2010) based on regional atmospheric climate modeling. *Geophysical Research Letters*, *39*, L04501. https://doi.org/10.1029/2011GL050713

Luthcke, S. B., Sabaka, T. J., Loomis, B. D., Arendt, A. A., McCarthy, J. J., & Camp, J. (2013). Antarctica, Greenland and Gulf of Alaska land-ice evolution from an iterated GRACE global Mascon solution. *Journal of Glaciology*, *59*(216), 613–631. https://doi.org/10.3189/2013JoG12J147

Medley, B., McConnell, J. R., Neumann, T. A., Reijmer, C. H., Chellman, N., Sigl, M., & Kipfstuhl, S. (2018). Temperature and snowfall in western Queen Maud Land increasing faster than climate model projections. *Geophysical Research Letters*, *45*(3), 1472–1480. https://doi.org/10.1002/2017GL075992

Mouginot, J., Rignot, E., & Scheuchl, B. (2014). Sustained increase in ice discharge from the Amundsen Sea Embayment, West Antarctica, from 1973 to 2013. *Geophysical Research Letters*, *41*, 1576–1584. https://doi.org/10.1002/2013GL059069
Nicolas, J. P., Vogelmann, A. M., Scott, R. C., Wilson, A. B., Cadeddu, M. P., Bromwich, D. H., et al. (2017). January 2016 extensive summer melt in West Antarctica favoured by strong El Niño. *Nature Communications*, *8*. https://doi.org/10.1038/ncomms15799
Palerme, C., Kay, J. E., Genthon, C., L'Ecuyer, T., Wood, N. B., & Claud, C. (2014). How much snow falls on the Antarctic ice sheet? *The Cryosphere*, *8*(4), 1577–1587. https://doi.org/10.5194/tc-8-1577-2014
Paolo, F. S., Padman, L., Fricker, H. A., Adusumilli, S., Howard, S., & Siegfried, M. R. (2018). Response of Pacific-sector Antarctic ice shelves to the El Niño/Southern Oscillation. *Nature Geoscience*, *11*(2), 121. https://doi.org/10.1038/s41561-017-0033-0
Pope, J. O., Holland, P. R., Orr, A., Marshall, G. J., & Phillips, T. (2017). The impacts of El Niño on the observed sea ice budget of West Antarctica. *Geophysical Research Letters*, *44*, 6200–6208. https://doi.org/10.1002/2017GL073414
Rignot, E., Jacobs, S., Mouginot, J., & Scheuchl, B. (2013). Ice-shelf melting around Antarctica. *Science*, *341*(6143), 266–270. https://doi.org/10.1126/science.1235798
Sasgen, I., Dobslaw, H., Martinec, Z., & Thomas, M. (2010). Satellite gravimetry observation of Antarctic snow accumulation related to ENSO. *Earth and Planetary Science Letters*, *299*(3), 352–358. https://doi.org/10.1016/j.epsl.2010.09.015
Scott, R. C., Nicolas, J. P., Bromwich, D. H., Norris, J. R., & Lubin, D. (2019). Meteorological drivers and large-scale climate forcing of West Antarctic surface melt. *Journal of Climate*, *32*(3), 665–684. https://doi.org/10.1175/JCLI-D-18-0233.1
Shepherd, A., Ivins, E. R., Geruo, A., Barletta, V. R., Bentley, M. J., Bettadpur, S., et al. (2012). A reconciled estimate of ice-sheet mass balance. *Science*, *338*(6111), 1183–1189. https://doi.org/10.1126/science.1228102
Shepherd, A., Ivins, E. R., Rignot, E., Smith, B., Van Den Broeke, M., Velicogna, I., et al. (2018). Mass balance of the Antarctic Ice Sheet from 1992 to 2017. *Nature*, *556*, 219–222. https://doi.org/10.1038/s41586-018-0179-y
Smith, S. A., Vosper, S. B., & Field, P. R. (2015). Sensitivity of orographic precipitation enhancement to horizontal resolution in the operational Met Office Weather forecasts. *Meteorological Applications*, *22*(1), 14–24. https://doi.org/10.1002/met.1352
Stuecker, M. F., Bitz, C. M., & Armour, K. C. (2017). Conditions leading to the unprecedented low Antarctic sea ice extent during the 2016 austral spring season. *Geophysical Research Letters*, *44*, 9008–9019. https://doi.org/10.1002/2017GL074691
Tedesco, M., & Monaghan, A. J. (2009). An updated Antarctic melt record through 2009 and its linkages to high-latitude and tropical climate variability. *Geophysical Research Letters*, *36* L18502. https://doi.org/10.1029/2009GL039186
Turner, J. (2004). The El Niño–Southern Oscillation and Antarctica. *International Journal of Climatology: A Journal of the Royal Meteorological Society*, *24*(1), 1–31. https://doi.org/10.1002/joc.965
van de Berg, W. J., & Medley, B. (2016). Brief communication: Upper-air relaxation in RACMO2 significantly improves modelled interannual surface mass balance variability in Antarctica. *The Cryosphere*, *10*(1), 459–463. https://doi.org/10.5194/tc-10-459-2016
van Wessem, J. M., Jan Van De Berg, W., Noël, B. P., Van Meijgaard, E., Amory, C., Birnbaum, G., et al. (2018). Modelling the climate and surface mass balance of polar ice sheets using RACMO2: Part 2: Antarctica (1979-2016). *The Cryosphere*, *12*(4), 1479–1498. https://doi.org/10.5194/tc-12-1479-2018
Walker, C. C., & Gardner, A. S. (2017). Rapid drawdown of Antarctica's Wordie Ice Shelf glaciers in response to ENSO/Southern Annular Mode-driven warming in the Southern Ocean. *Earth and Planetary Science Letters*, *476*, 100–110. https://doi.org/10.1016/j.epsl.2017.08.005
Watkins, M. M., Wiese, D. N., Yuan, D. N., Boening, C., & Landerer, F. W. (2015). Improved methods for observing Earth's time variable mass distribution with GRACE using spherical cap Mascons. *Journal of Geophysical Research: Solid Earth*, *120* 2648–2671. https://doi.org/10.1002/2014JB011547
Wiese, D. N., Landerer, F. W., & Watkins, M. M. (2016). Quantifying and reducing leakage errors in the JPL RL05M GRACE Mascon solution. *Water Resources Research*, *52* 7490–7502. https://doi.org/10.1002/2016WR019344
Yuan, X., & Li, C. (2008). Climate modes in southern high latitudes and their impacts on Antarctic sea ice. *Journal of Geophysical Research*, *113*, C06S91. https://doi.org/10.1029/2006JC004067
Zwally, H. J, Giovinetto, M. B., Beckley, M. A., & Saba, J. L. (2012). *Antarctic and Greenland drainage systems, GSFC Cryospheric Sciences Laboratory*. Retrieved from https://icesat4.gsfc.nasa.gov/cryo_data/ant_grn_drainage_systems.php

Erratum

In the originally published version of this article, in the next-to-last sentence of section 2.2, “three estimates averaged” should have read “five estimates averaged.” This error has since been corrected, and the present version may be considered the authoritative version of record.